

MULTISENSOR RASTER AND VECTOR DATA FUSION BASED ON UNCERTAINTY MODELING

Sang-Chul Lee and Peter Bajcsy

National Center for Supercomputing Applications
University of Illinois at Urbana-Champaign
{sclee,pbajcsy}@ncsa.uiuc.edu

ABSTRACT

We propose a new methodology for fusing temporally changing multisensor raster and vector data by developing a spatially and temporally varying uncertainty model of acquired and transformed multisensor measurements. The proposed uncertainty model includes errors due to (1) each sensor by itself, e.g., sensor noise; (2) transformations of measured values to obtain comparable physical entities for data fusion and/or to calibrate sensor measurements; (3) vector data spatial interpolation that is needed to match different spatial resolutions of multisensor data; and (4) temporal interpolation that has to take place if multisensor acquisitions are not accurately synchronized. The proposed methodology was tested using simulated data with varying (a) amount of sensor noise, (b) spatial offset of point sensors generating vector data and (c) model complexity of the underlying physical phenomenon. We demonstrated the multisensor fusion approach with a data set from a structural health monitoring application domain.

1. INTRODUCTION

There exist multiple definitions of data fusion [1]. The data fusion, as defined in this paper, is understood as the process of integrating multisensor data for an end user in such a manner that the user is able to retrieve the most accurate measurement, its uncertainty, and the associated sensor by specifying (1) a physical entity, (2) a spatial location, and (3) a time from the list of physical related variables and measured range of spatial and temporal intervals.

The multisensor data fusion problem as defined above occurs in most scientific measurements consisting of multiple instruments that collect spatially overlapped data simultaneously. Our focus is on a specific problem of raster and vector data fusion that can be found in several domains and instrumentation systems, such as geographic information systems (GIS) [2], hazard monitoring systems [3][4], aircraft navigation [4], and structural and earthquake engineering tests. The application driver for this work is the analysis of displacement measure-

ments¹ and photoelastic-based strain raster measurements² for material structural health assessment in earthquake.

In general, multisensor data fusion is motivated by (1) reducing overall redundant information from different sensors, (2) increasing information gain due to the utilization of multiple sensors, and (3) increasing the accuracy and decreasing the uncertainty of the system. Furthermore, multisensor data fusion can provide additional benefits such as the extended temporal and spatial coverage, reduced ambiguity, enhanced spatial resolution, and increased dimensionality of the measurement space.

The problem of multisensor raster and vector data fusion is formulated as follows. Given a set of spatially dense raster measurements of a physical entity λ_r^{input} and a set of spatially sparse point measurements λ_v^{input} that are observations of the same phenomenon at the same spatial location and time, find the most accurate measurements of a comparable physical entity λ^{output} , its uncertainty, and the corresponding sensor at any observed location and time.

In order to solve the multisensor data fusion problem as formulated, one has to overcome input data heterogeneity first and then analyze the spatial and temporal accuracy of comparable entities derived from multiple sensor measurements. The multisensor input data heterogeneity occurs due to different (1) sensor coordinate systems, (2) temporal sampling (synchronization), (3) measured variables, and (4) data types (raster versus vector). These data heterogeneities can be resolved by (1) finding coordinate system transformations to register data sets [6], (2) identifying a common time instance and applying temporal resampling, (3) performing analytical transformations of measured variables, and (4) fitting spatial interpolation/extrapolation models [7] and applying spatial resampling [8]. Although resolving data heterogeneities is necessary for data fusion, each data operation changes uncertainty associated with a spatial and a temporal sensor measurement, and hence, uncertainty modeling has to include all data processing steps.

¹ Krypton System (<http://www.krypton.be>).

² Stress Photonics System (<http://www.stressphotonics.com>).

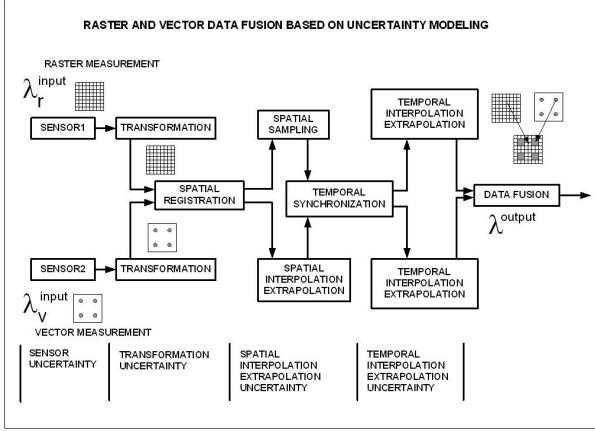


Figure 1: An overview of raster and vector data fusion process and associated uncertainty model components.

We propose a methodology for modeling and estimating sensor data uncertainty that includes all raster and vector data fusion steps. The proposed uncertainty model is composed of error contributions due to (1) each sensor by itself, e.g., sensor noise; (2) transformations of measured values to obtain comparable physical entities for data fusion and/or to calibrate sensor measurements; (3) vector data spatial interpolation that is needed to match different spatial resolutions of multisensor data; and (4) temporal interpolation that has to take place if multisensor acquisitions are not accurately synchronized. The global uncertainty model ε is presented in Equation (1) below, where λ^{input} is a set of *measured* physical entities:

$$\varepsilon(\mathbf{x}, t, \lambda^{input}) = f(\varepsilon^{SENSOR}(\lambda^{input}), \varepsilon^{TRANSFORMATION}(\lambda^{input}, \psi(\lambda^{input})), \varepsilon^{SPATIAL ADJUSTMENT}(\mathbf{x}), \varepsilon^{TEMPORAL ADJUSTMENT}(t)), \quad (1)$$

where \mathbf{x} is a spatial location in the local coordinate system, t is a time frame, ψ is a variable transformation function, and f is a function of the order of the data fusion steps.

The fusion of raster and vector data is performed by minimizing the uncertainty of measurements λ_i^{input} at any spatial location \mathbf{x} and a time instance t after performing all necessary transformations ψ_i to obtain comparable physical entities (see Equation (2) below):

$$\lambda^{output}(\mathbf{x}, t) = \psi_{\hat{i}}(\mathbf{x}, t, \lambda_{\hat{i}}^{input}), \quad (2)$$

$$\hat{i} = \arg \min_i (\varepsilon_i(\mathbf{x}, t, \lambda_i^{input}))$$

where $\lambda_i^{input} \in \lambda^{input}$, $0 \leq i \leq \text{number of sensors}$, λ_i^{input} are different input physical entities and each linear function ψ_i associated with λ_i^{input} converts the input entity to a comparable (output) physical entity that is to be fused into λ^{output} . The raster and vector data fusion process is illustrated in Figure 1 as it resolves input data heterogeneity issues. Figure 1 also shows the uncertainty model components associated with each processing step of the

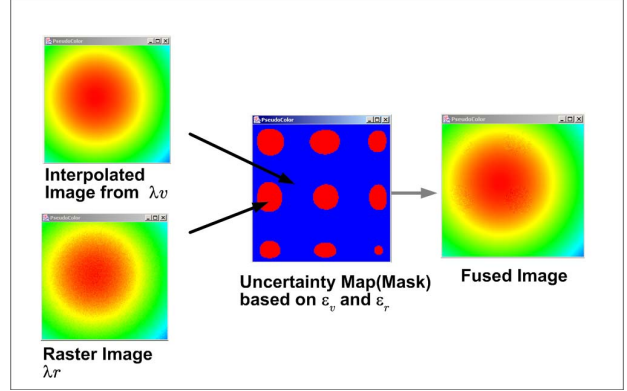


Figure 2: Data fusion process with an uncertainty map.

data fusion process. While some of the processing steps can occur multiple times during data fusion (for instance, vector data transformation before and after spatial registration), other processing steps might occur only with raster or vector data but not both (for example, spatial interpolation of vector data or spatial sampling of raster data).

The paper is organized as follows. Section 2 describes our analytically derivation of the uncertainty components in Equation (1). Next, Section 3 presents the data fusion results obtained from simulated experiments to demonstrate the theoretical uncertainty model. The paper is summarized in Section 4.

2. UNCERTAINTY MODEL FOR RASTER AND VECTOR DATA FUSION

The fusion rule for raster and vector data can be presented as follows:

$$\lambda^{output}(\mathbf{x}, t) = \begin{cases} \lambda_v^{output}(\mathbf{x}, t) : \text{if } \varepsilon_r(\mathbf{x}, t, \lambda_r^{input}) > \varepsilon_v(\mathbf{x}, t, \lambda_v^{input}) \\ \lambda_r^{output}(\mathbf{x}, t) : \text{otherwise} \end{cases} \quad (3)$$

where λ_r and λ_v are the raster and vector data values in the *registered* coordinate system, ε_r and ε_v represent the uncertainty of the *interpolated* vector data and the raster data, respectively. Using uncertainty models for ε_v and ε_r and the fusion rule in Eq. (3), we can create a mask shown in Figure 2. This image mask (or uncertainty map) shows the regions that contain measurements with the lowest uncertainty from vector and raster sensors (red circular shapes in the image mask denote smaller uncertainty in raster data).

For simplicity, we model the uncertainty distribution ε_r of raster data by only the sensor noise component $\varepsilon^{SENSOR}(\lambda^{input})$ in Equation (1). The sensor noise follows a Gaussian distribution with zero mean and standard deviation ω_r according to Equation (4):

$$\varepsilon_r = \varepsilon_r(\mathbf{x}, t, \lambda_r^{input}) = n_r, \text{ where } n_r \sim N(0, \omega_r) \quad (4)$$

Our model for the uncertainty distribution ε_v of vector data includes dependencies on (1) spatial location \mathbf{x} and time t , (2) physical model of the measured phenomenon $M^P(\mathbf{x}, t, \beta^P)$ (β^P is a physics-based descriptor), (3) sensor noise n_v , and (4) spatial and temporal interpolation descriptors $I^S(S, \beta^{SI})$, $I^T(S, \beta^{TI})$ with S denoting a set of data points and β^{SI} and β^{TI} denoting interpolation model descriptors. Thus, the uncertainty model ε_v and the interpolated vector data λ_v are defined as follows:

$$\varepsilon_v = \varepsilon_v(\mathbf{x}, t, M^P, I^S, I^T, n_v) \quad (5)$$

$$\lambda_v = I^S(S, \beta^{SI}) \quad (6)$$

To simplify our mathematical derivation, we assume that (a) measurements are temporally *synchronized*; (b) sensor noise n_v follows Gaussian distribution according to Equation (7) and is smaller than the raster sensor noise ($\omega_v < \omega_r$); (c) M^P , defined in Equation (8), corresponds to smoothly distributed physical entities measured on a test object (e.g., structure with no cracks); (d) β^{SI} and β^{TI} are *uniform cubic B-spline* models [9] that have been proved to be superior to other methods with similar cost [10]; and (e) S is a set of uniformly distributed points described in Equation (9):

$$\varepsilon_v^{\text{SENSOR}}(\lambda_v^{input}) = n_v; \quad n_v \sim N(0, \omega_v) \quad (7)$$

$$M^P = G(\mathbf{x}, \sigma) = e^{-\frac{\mathbf{x}_x^2 + \mathbf{x}_y^2}{2\sigma_{ref}^2}} \quad (8)$$

$$\begin{aligned} S &= S(\mathbf{x}_{init}, \xi, t_{init}, \tau, M^P, n_v) \\ &= \{s_{ij}^k \mid s_{ij}^k = M^P(\mathbf{x}_{ij}, t) + n_v\} \end{aligned} \quad (9)$$

where $\mathbf{x}_{ij} = \mathbf{x}_{init} + (i\xi_x, j\xi_y)$, $t = t_{init} + k\tau$ and \mathbf{x}_{init} is the origin in the local coordinate system, ξ is sensor spacing, t_{init} is initial temporal sequence and τ is temporal difference. Then, the final spatially adjusted variable is modeled as:

$$\begin{aligned} \lambda_v &= I^S(S(x_{init}, \xi, t_{init}, \tau, (\beta^P = G), n_v), (\beta^{SI} = \text{B-spline})) \\ &= \bigcup_k Q_k(u, v, P(S, \beta^{SI})) \end{aligned} \quad (10)$$

where Q_k is an interpolated patch, $0 \leq u, v \leq 1$, and P is a set of control points that are derived from a set of data points S .

The uncertainty from variable transformations comes from linear computations (ψ_i) to obtain a new physical entity λ^{output} , e.g., addition, subtraction, and multiplication. This uncertainty component $\varepsilon^{\text{TRANSFORMATION}}(\lambda^{input}, \psi(\lambda^{input}))$ is known as *error propagation* [11].

The uncertainty from spatial adjustment in Equation (1) will include the described uncertainty from variable transformations for interpolation and its own uncertainty

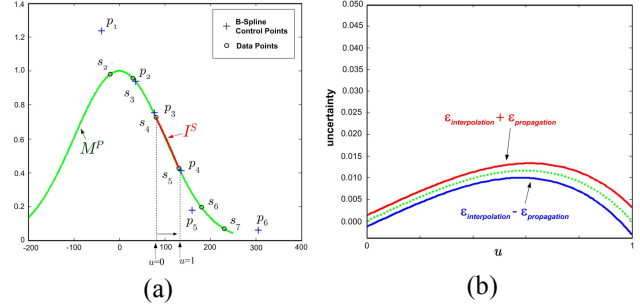


Figure 3: An example of reference and interpolated curves (Eq. (12) and (13)) and (b) uncertainty between s_4 and s_5 (Eq. (14)).

due to interpolation model characteristics. This uncertainty is presented in Equation (11):

$$\varepsilon^{\text{SPATIAL ADJUSTMENT}} = \|M^P - I^S\| = \varepsilon_{\text{interpolation}} \pm \varepsilon_{\text{propagation}} \quad (11)$$

3. RESULTS OF DATA FUSION USING UNCERTAINTY MAPS

We conducted simulations of data fusion using uncertainty maps in order to demonstrate the accuracy of the *mathematically* predictable *nonuniform uncertainty map*. For the temporal and spatial simulations, we used 1D and 2D B-spline models. In the 1D case, the reference curve M^P between points s_4 and s_5 is defined as:

$$M^P(u, S) = \exp\left(-\frac{(u\xi + s_4)^2}{2\sigma_{ref}^2}\right), 0 \leq u \leq 1 \quad (12)$$

Using B-spline data fitting methods [9], the interpolated data are modeled as a cubic polynomial function:

$$I^S(u, S) = \sum_{i=0}^3 a_i u^i \pm n_v \cdot \sqrt{\sum_{i=0}^3 b_i u^{2i}}, 0 \leq u \leq 1 \quad (13)$$

where a_i and b_i are coefficients. Then the uncertainty with respect to different spatial locations u ($0 \leq u \leq 1$) is represented as

$$\begin{aligned} \varepsilon^{\text{SPATIAL ADJUSTMENT}}(u) &= \\ &= \left| \exp\left(-\frac{(u\xi + s_4)^2}{2\sigma_{ref}^2}\right) - \sum_{i=0}^3 a_i u^i \right| \pm n_v \cdot \sqrt{\sum_{i=0}^3 b_i u^{2i}} \end{aligned} \quad (14)$$

Figure 3(a) shows the reference curve M^P , sampled data points s_i , B-spline control points p_i and the interpolated curve I^S in the simulated results. Figure 3(b) shows the uncertainty due to the spatial adjustments as in Equation (14). The results show that the uncertainty reaches maximum in the middle of two adjacent points $u \approx 0.6$ and the variation of the uncertainty (gap between two solid curves in Figure 3(b)) is larger for higher u .

In the 2D case, the reference patch, surrounded by the data points $s_{33}, s_{34}, s_{44}, s_{43}$, is defined as:

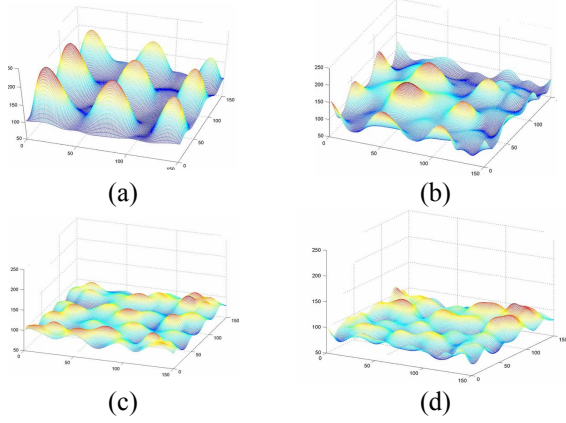


Figure 4 : Error maps for sensor spacing ξ set to (a) 50, (b) 45, (c) 40, and (d) 35 (pixels). x and y axes represent the pixel coordinates of the interpolated image, and the z -axis shows the standard error $\varepsilon_v(\mathbf{x}, \lambda_v)$.

$$M^P(u, v, S) = \exp\left(-\frac{(u\xi_x + s_{33x})^2 + (v\xi_y + s_{33y})^2}{2\sigma_{ref}^2}\right) \quad (15)$$

The interpolated patch I^S is represented as a cubic polynomial function $Q(u, v, S)$ as shown below:

$$I^S(u, v, S) = \sum_{i=0}^3 \sum_{j=0}^3 a_{ij} u^i v^j \pm n_v \cdot \sqrt{\sum_{i=0}^3 \sum_{j=0}^3 b_{ij} u^{2i} v^{2j}} \quad (16)$$

where a_{ij} and b_{ij} are coefficients that were calculated from the data points S . For the 2D analysis, we calculated an uncertainty distribution $\varepsilon^{\text{SPATIAL ADJUSTMENT}}$ by generating $n(=100)$ sets of vector data and quantitatively evaluated by the sum of squared errors:

$$\begin{aligned} \varepsilon^{\text{SPATIAL ADJUSTMENT}}(u, v) &= \sqrt{\frac{1}{n} \sum_1^n (M^P(u, v, S) - I^S(u, v, S))^2} \quad (17) \end{aligned}$$

Figures 4(a), (b), (c), and (d) show the uncertainty distribution with different vector sensor spacing ξ , each formed by nine joined patches from 4 by 4 vector measurements. The average of all peaks decreases with smaller ξ (denser point measurements), which means the denser vector data produce the lower uncertainty variation (from spatial adjustment) in the interpolated image.

4. SUMMARY

In this paper, we have developed a new methodology for fusing multisensor raster and vector data using uncertainty models. Our fusion approach is based on selecting those temporally and spatially changing measurements that minimize the uncertainty or maximize the accuracy of each measurement. We have investigated uncertainty

models for raster and vector data as a function of errors occurring due to (1) sensor noise, (2) transformations of measured values to obtain comparable physical entities for data fusion and/or to calibrate sensor measurements, (3) vector data spatial interpolation/extrapolation to match different spatial resolutions of multisensor data, and (4) temporal interpolation/extrapolation to match asynchronous multisensor acquisitions. While decomposing the uncertainty model into components corresponding to individual data fusion operations, we simulated functional dependencies of uncertainty model components with respect to (a) spatial offset of point sensors generating vector data, (b) amount of sensor noise, and (c) curvature variation representing the complexity of underlying measured phenomena. Our future work will focus on optimizing the design of real experiments, for example, vector sensor spacing, raster sensor resolution, based on our mathematical model.

5. REFERENCES

- [1] D. Hall and J. Llinas, "An introduction to multisensor data fusion," *IEEE Proceedings: Special Issue on Data Fusion*, 85(1), January 1997.
- [2] W. A. Flugel and B. Muschen, "Applied remote sensing and GIS integration for model parameterization (ARSGISIP)," *The 27th International symposium on Remote Sensing of Environment*, Tromso, Norway, pp.354-357, June 8-12, 1998.
- [3] Z. Chenghu and D. Yunyan, "Method and model for automatically extracting flood extent from NOAA AVHRR image on basis of knowledge," *Journal of Natural Disaster*, 6(4):100-108, 1997.
- [4] P. Bajcsy and S. Saha, "A new thermal infrared camera calibration approach using wireless MEMS sensors," *CNDS 2004*, San Diego, CA, Jan. 19-22 2004.
- [5] B.T. Sweet and C. Tiana, "Image Processing and Fusion for Landing Guidance," *In Enhanced and Synthetic Vision, Proceedings of SPIE*, volumn 2736, 1996.
- [6] J. R. Bergen and P. J. Burt, "A three-frame algorithm for estimating two-component image motion," *IEEE Transactions on Pattern Analysis and Machine Intelligence*, 14(9):886-896, September 1992.
- [7] M. A. Burgess, T. Chang, D. E. Dunford, R. H. Hoh, W. F. Home, R. F. Tucker, and J. A. Zak, "Synthetic vision technology demonstration: Flight tests," *Technical Report Research and Development Service*, Washington D.C. December 1993.
- [8] R. R. Schultz and R. L. Stevenson, "Extraction of high-resolution frames from video sequences," *IEEE Transactions on Image Processing*, June 1996.
- [9] A. Watt and M. Watt, "Advanced animation and rendering techniques," Addison-Wesley, Workingham, England, 1992.
- [10] P. Thévenaz, T. Blu, and M. Unser, "Image interpolation and resampling," *Handbook of Medical Image Processing*, in press, 1999.
- [11] J. Taylor, "An introduction to error analysis: the study of uncertainties in physical measurements," *University Science Books*, 1982.